Simulations of Three-dimensional Ciliary Beats and Cilia Interactions

Shay Gueron* and Nadav Liron
Department of Mathematics, Technion, Israel Institute of Technology, Haifa 32000, Israel

ABSTRACT A new set of equations describing the time evolution of torsion and curvature for an inextensible curve is developed. Combined with our recently developed Slender Body Theory approach to such problems, these equations were applied to simulate three-dimensional ciliary beats, while allowing for cilia interactions.

The computer animation technique, which was originally designed to display two-dimensional beats, has been enhanced to accommodate the new three-dimensional results.

INTRODUCTION

The simulations of ciliary and flagellar beats have attracted a great deal of research efforts, and considerable advance has been achieved in modeling procedures (1–5, 7, 27–29, and others). Due to typical dimensions, the motion of cilia and flagella in the (highly viscous and incompressible) surrounding fluid is governed by the Stokes equations. Additionally, no-slip boundary conditions on the surfaces (i.e., the velocity of the fluid on a cilium's surface, must match the velocity of the surface), and the condition of vanishing fluid disturbance at infinity must also be satisfied. The slenderness of cilia and flagella, and the properties of Stokes flows enabled a simplifying approximation, known as the Resistive Force Theory. This approach, pioneered by Gray and Hancock (10) has been used in many of the researches on the subject, with various resistance coefficients. Finer hydrodynamic analyses such as the Slender Body Theory and the Boundary Element Method have since been developed and applied to different problems involving flagellar motion with and without an attached cell body (e.g., refs. 9, 12–14, 21, 24–26). A refined approach to the modeling of ciliary motion was suggested in a recent paper by Gueron and Liron (11) (G-L henceforth). This enabled us to accurately simulate beats as dynamic problems, and to extend the applicability to multicilia configurations. This approach is used in this paper as well.

In nature, cilia, more often than not, beat in three-dimensional patterns. Nevertheless, none of the above mentioned works on the subject offered a three-dimensional (3-D) *dynamic model*. Some works on the 3-D mechanics of cilia and flagella were published by Hines and Blum (18–20) who dealt only with static problems, ignoring hydrodynamic effects. Other publications, as mentioned above, dealt with simulations of helical motions of flagella. Such motions are of a very specific and limited form of 3-D motions, and from a kinematic point of view, they are actually planar. Even in G-L, simulations were two-dimensional (2-D), although the main theorem used there is suitable for 3-D motions. The reason for modeling only 2-D beats was that the geometric equations for the propagation of 3-D curves were not available.

A planar curve can be determined by means of one parameter (its curvature for example). In many cases it is convenient to parameterize a 2-D curve by using the angle between its tangent and the horizontal axis (the derivative of which is the curvature). Indeed, this is the way (2-D) curves were parameterized in most of the previous models. One advantage of this parameterization is that the inextensibility condition (i.e., that the cilium maintains a constant length), which is required for ciliary motion simulations (18), is satisfied automatically. In three space dimensions, two (local) parameters are needed to describe a curve. In contrast to the two-dimensional case (15), the inextensibility condition cannot be satisfied automatically.

The dynamics of 3-D curves have been investigated in other contexts as well. Samuels and Donnelli (30) reported on the numerical propagation of 3-D vortex lines. Their straightforward approach suffered from stability problems. As a result they had to resort to extremely small time steps, and consequently, to the use of a supercomputer.

The problem of simulating 3-D ciliary motions, in reasonable time, is addressed in this paper. In the Preliminaries section we introduce several useful notations and quote the force-velocity relations that were developed in G-L. In the Modeling section, all the necessary equations for 3-D motion are developed. These equations enable the propagation (in time) of the curvature and the torsion along a 3-D curve, given its velocity distribution. This approach decreases the number of equations to be propagated from three, for the straightforward method, to two. In addition, its numerical implementation proves to be stable for relatively large time steps. In the Modeling section we also show how to satisfy the inextensibility condition. As in the 2-D models, the components of the internal force developed by the cilia are not independent of each other. The appropriate relation between these components (which is a generalization of the analogous relation for 2-D motion (Hines and Blum (15) (H-B henceforth) and G-L) is derived in the Modeling section below.

Combining the 3-D version of G-L's force-velocity relation with the new geometric equations yields a 3-D dynamic model, which is suitable for simulating the motion of either an isolated cilium or several interacting cilia.

Received for publication 29 June 1992 and in final form 12 March 1993.

*Currently at the Center for Applied Mathematics, 504 ETC Building, Cornell University, Ithaca, NY 14853

0006-3495/93/07/499/09 $2.00

As a result of extending the model to three spatial dimensions, a third (binormal) component of the shear force is introduced into the equations describing the internal mechanism (in addition to the normal and the tangential ones). The existence of this component enables the driving of the cilium out of the plane, thus producing the 3-D motion. Appropriate consideration is given to the way the elastic properties of the cilium are reflected in the 3-D motion. The chosen "engine" (internal mechanism) produced beat patterns that resemble actual beats. Following G-L, the model and its numerical implementation are organized in a modular way, in order to allow easy application with different internal mechanisms.

The precise choice of the parameters used for the simulations and a brief description of the numerical methods are also detailed in the Modeling section. In the Results section we present results of modeling a single cilium and several interacting cilia and conclude with a short discussion.

PRELIMINARIES

In order to make our paper shorter and clearer we adopt several notations and conventions that will be used henceforth. These notations are consistent with those used in G-L, which makes the 2-D and 3-D cases convenient to compare.

Methods

The cilium is modeled as an inextensible (i.e., maintaining constant length) cylindrical filament of length L. The centerline of the filament is a curve, parameterized by its arclength parameter s ($0 \le s \le L$: $s = 0$ at the "anchor" where the cilium is attached to a surface, and $s = L$ at the distal free end).

We define the three axes as x_1, x_2, and x_3 in Fig. 1 *a* and set $x_3 = 0$ at the cilium's anchor. Whenever dealing with a single cilium, its anchor is located at the origin. The location of the anchors for multicilia configurations will be specified in the examples.

At each point on the cilium (curve) we refer to two sets of coordinates. The first one represents the (global) location (x_1,x_2,x_3) (with respect to some fixed origin), and the other is the local Frenet Trihedron $[\mathbf{T}(s,t),\mathbf{N}(s,t), \mathbf{B}(s,t)]$ (tangential, normal, and binormal unit vectors, respectively).

The subscripts T, N, and B denote the tangential, normal, and binormal components of vectors, respectively, and the subscripts s and t denote partial differentiation with respect to s and to the time, t, respectively. We denote by $\mathbf{x}_1$, $\mathbf{x}_2$, and $\mathbf{x}_3$ the three unit vectors in the direction of x_1, x_2, and x_3, respectively.

$\epsilon = a/L$, the ratio of the radius of the cilium (a) to its length (L), is defined as the slenderness parameter. It is assumed that $\epsilon \ll 1$.

We use $\mathbf{F}(s,t)$ ($=\mathbf{F}$) to denote the shear force developed by the internal mechanism of the cilium, and $\boldsymbol{\phi}(s,t)$ ($=\boldsymbol{\phi}$) for the force per unit of length (i.e., drag force) exerted *on* the cilium by the surrounding fluid in which the cilia beat. $\mathbf{V}(s,t)$ ($=\mathbf{V}$) is the velocity of the cross section s, and μ is the viscosity of the surrounding fluid. κ and τ denote the curvature and the torsion of the cilium, respectively.

The theoretical basis for modeling the motion of a cilium is the theorem connecting the drag force and the velocity stated and proved in G-L. We quote this theorem here again as follows.

Theorem 1

Let $\mathbf{r}(s,t)$ be the location of the centerline of a cilium ($0 \le s \le L$) of radius a, attached to a flat surface at $x_3 = 0$. We use the following notations for any two location vectors $\mathbf{r}$ and $\mathbf{r}_0$ and intensity vector $\boldsymbol{\phi}$ (see G-L for explicit expressions):

$\mathbf{U}^s(\mathbf{r},\mathbf{r}_0,\boldsymbol{\phi})$ = the velocity, induced at $\mathbf{r}$, by a Stokeslet with intensity $\boldsymbol{\phi}$, located at $\mathbf{r}_0$ (in infinite medium). $\mathbf{U}^{si}(\mathbf{r},\mathbf{r}_0,\boldsymbol{\phi})$ = the velocity, induced at $\mathbf{r}$, by a Stokeslet located at $\mathbf{r}_0$, with intensity $\boldsymbol{\phi}$, *and* by its image system (i.e., this is a basic solution satisfying no-slip conditions at $x_3 = 0$). $\mathbf{U}^d(\mathbf{r},\mathbf{r}_0,\boldsymbol{\phi})$ = the velocity, induced at $\mathbf{r}$, by a Doublet with intensity $\boldsymbol{\phi}$, located at $\mathbf{r}_0$ (in infinite medium). $\mathbf{U}^{di}(\mathbf{r},\mathbf{r}_0,\boldsymbol{\phi})$ = the velocity, induced at $\mathbf{r}$, by a Doublet, located at $\mathbf{r}_0$, with intensity $\boldsymbol{\phi}$, *and* by its image system (i.e., this is a basic solution satisfying no-slip conditions at $x_3 = 0$). $\mathbf{V}^{si}(\mathbf{r},\mathbf{r}_0,\boldsymbol{\phi}) = \mathbf{U}^{si}(\mathbf{r},\mathbf{r}_0,\boldsymbol{\phi}) - \mathbf{U}^s(\mathbf{r},\mathbf{r}_0,\boldsymbol{\phi})$ (i.e., the velocity induced by the image system only). $\mathbf{V}^{si}(\mathbf{r},\mathbf{r}_0,\boldsymbol{\phi}) = \mathbf{U}^{di}(\mathbf{r},\mathbf{r}_0,\boldsymbol{\phi}) - \mathbf{U}^d(\mathbf{r},\mathbf{r}_0,\boldsymbol{\phi})$ (No-slip conditions imply here vanishing velocities on the plane $x_3 = 0$.)

Let $q = O(a/\sqrt{\epsilon})$ and $q < s_0 < L - q$ (see Fig. 1 *b*). If $\mathbf{V}(s_0,t)$ is the velocity of the cross section s_0 then:

$$\mathbf{V}(s_0,t) = -(1/C_T)\phi_T(s_0,t)\mathbf{T} - (1/C_N)\phi_N(s_0,t)\mathbf{N} - (1/C_B)\phi_B(s_0,t)\mathbf{B}$$
$$+ \int_{|s-s_0|>q} \mathbf{U}^s[\mathbf{r}(s,t),\mathbf{r}(s_0,t),-\boldsymbol{\phi}(s,t)]\,ds$$
$$+ \int_{0\le s\le L} \{\mathbf{V}^{si}[\mathbf{r}(s,t),\mathbf{r}(s_0,t),-\boldsymbol{\phi}(s)] + \mathbf{V}^{di}[\mathbf{r}(s,t),\mathbf{r}(s_0,t),-(a^2/4\mu)\boldsymbol{\phi}(s,t)]\}\,ds$$
$$+ \mathbf{V}_{ext}(s_0,t) + 0(\sqrt{\epsilon}) \qquad (1)$$

where

$$C_T = \frac{8\pi\mu}{-2 + 4\ln(2q/a)}, \qquad C_N = C_B = \frac{8\pi\mu}{1 + \ln(2q/a)}. \qquad (2)$$

The term $\mathbf{V}_{ext}(s_0)$ represents the external flow field that is induced (at s_0) by sources other than moving segments of the cilium (neighboring cilia for example). It is assumed that $\mathbf{V}_{ext}(s_0)$ does not change significantly on the scale of a.

To present the relation (Eq. 1) as an integral equation for the drag force, define

$$\mathbf{G}(s_0,t) = \int_{|s-s_0|>q} \mathbf{U}^s[\mathbf{r}(s,t),\mathbf{r}(s_0,t),-\boldsymbol{\phi}(s,t)]\,ds$$
$$+ \int_{0\le s\le L} \{\mathbf{V}^{si}[\mathbf{r}(s,t),\mathbf{r}(s_0,t),-\boldsymbol{\phi}(s)] + \mathbf{V}^{di}[\mathbf{r}(s,t),\mathbf{r}(s_0,t),-(a^2/4\mu)\boldsymbol{\phi}(s,t)]\}\,ds$$
$$+ \int_{\substack{0\le s\le L \\ \text{neighboring cilia}}} \mathbf{U}^s[\mathbf{r}(s,t),\mathbf{r}(s_0,t),-\boldsymbol{\phi}(s,t)]\,ds \qquad (3)$$

and $g_N = C_N G_N$, $g_T = C_T G_T$, $g_B = C_B G_B$.

Here, $\mathbf{G}(s_0,t)$ represents the *velocity* induced at s_0 by the "far" segments, while $\mathbf{g}(s_0,t)$ represents the induced *drag force* per unit of length.

Note that the interactions with the neighboring cilia is included in the last term of Eq. 3.

The force-velocity relation becomes:

$$\phi_N = -C_N V_N + g_N, \qquad \phi_T = -C_T V_T + g_T,$$
$$\phi_B = -C_B V_B + g_B. \qquad (4)$$

In order to make our equations non-dimensional we introduce the normalized variables $s^* = s/L$, $t^* = \omega t$, $S^* = S/S_0$, where ω is a typical frequency, L is the length of the cilium, and S_0 is a typical magnitude of shear force. All of the following equations in the paper appear in their non-dimensional form and the asterisks are dropped. The specific choices for ω, L, and S_0 are discussed in the following section.

MODELING: THE EQUATIONS OF MOTION, THE INTERNAL MECHANISM, THE INITIAL AND BOUNDARY CONDITIONS, AND THE NUMERICAL METHODS

In this section we describe the modeling of the cilium's internal mechanism and the equations needed to simulate its 3-D motion.

Geometric equations relating the curvature, the torsion, and the velocity

We present here a system of equations relating the components of the local velocity to the geometric variables that describe the curve (i.e., the cilium). The need for these equations precluded until now simulations of 3-D beats. The cilium is described by using its arclength parameter. The *local* curvature and torsion (both expressed as functions of the arclength) define the centerline of the cilium uniquely. This is achieved by integrating the Frenet equations (32) with respect to s, combined with the orientation and the location at $s = 0$ (serving as boundary conditions) as follows.

$$\mathbf{T}_s = \kappa\mathbf{N}, \qquad \mathbf{B}_s = -\tau\mathbf{N}, \qquad \mathbf{N}_s = \tau\mathbf{B} - \kappa\mathbf{T}. \tag{5}$$

An analogous parameterization was used in the 2-D case. The difference is that to describe a planar curve a single parameter (e.g., $\alpha = \kappa_s$) is sufficient.

The motion, *in time*, of an *inextensible* curve can be described using the following theorem.

Theorem 2

Let $V_T(s)$, $V_N(s)$, and $V_B(s)$ be the (local) velocity components of each point along an inextensible curve. The equations describing the evolution of the curvature and the torsion in time are:

$$\kappa_t = V_{Nss} + V_T\kappa_s - 2\tau V_{Bs} - \tau_s V_B + (\kappa^2 - \tau^2)V_N, \tag{6}$$

$$\tau_t = \beta_s + \kappa(V_{Bs} + \tau V_N), \tag{7}$$

where β is defined by

$$\beta\kappa = V_{Bss} + 2V_{Ns}\tau + V_N\tau_s + V_T\kappa\tau - V_B\tau^2. \tag{8}$$

We make here some short comments and leave the complete proof to Appendix A. The proof of the theorem is straightforward. The essence is to cross-differentiate the location vector, $\mathbf{r}(s)$, with respect to s and to t. Since the curve is inextensible, each point is uniquely attributed to a specific value of s for all t. One can therefore interchange the order of the differentiation to obtain the following identity:

$$\mathbf{r}(s,t)_{st} = \mathbf{T}_t = \mathbf{r}(s,t)_{ts} = \mathbf{V}_s. \tag{9}$$

Decomposing Eq. 9 into its components and using the fact that $|\mathbf{T}| = |\mathbf{N}| = 1$ completes the proof.

We conclude about cases where $\kappa(s) = 0$ at one or more points along the curve. Equations 6–8 cannot be applied to such cases since β is not determined from Eq. 8. However, this is not surprising, as a 3-D straight line does not possess an intrinsic set of three orthogonal unit vectors $\mathbf{T}$, $\mathbf{N}$, and $\mathbf{B}$ (due to the fact that a straight segment does not define a unique plane, and hence no unique normal vector may be attributed to it).

Modeling the internal mechanism of the cilia

Three equations for the three components of the internal (shear) force developed in the cilium are to be determined in order to model its internal mechanism. Unlike the 2-D case, we cannot simply adopt acceptable concepts from other mechanisms that appear in the literature (as we did in G-L), since they all deal with 2-D motions and therefore consist of only two components. An equation for the third component, namely the binormal shear force (F_B), must be introduced to the model. However, we still model the normal component (F_N) the same way as in G-L (with only slight modifications). We first show that the inextensibility constraint and the force balance (see Eqs. B2–B5) determine the tangential force F_T as a function of F_N and F_B. This is the generalization of the analogous equation in G-L (where the normal component F_T is expressed as a function of F_N).

Assertion

The inextensibility requirement dictates the following equation:

$$F_{Tss} = (1 + C_{TN})F_{Ns}\kappa + C_{TN}F_T\kappa^2 + F_N\kappa_s - C_{TN}g_N\kappa + g_{Ts} - C_{TN}\kappa\tau F_B, \tag{10}$$

where $C_{TN} = C_T/C_N$. We leave the proof to Appendix B.

This paper serves mainly as an example for modeling 3-D motion, and thus we are not interested in a specific internal mechanism. Consequently, we use a rather artificial mechanism which we call a "load-dependent engine." By this we mean that the engine is composed of two contributions: one is the actual actively generated force, and the other is the passive elastic resistance of the cilium. special consideration should be given to the proper way the elastic resistance is introduced.

As in G-L, the normal component of the shear force, F_N, is defined by

$$F_N = E_b\kappa_s + S(s,t). \tag{11}$$

The first term, being proportional to the curvature's gradient, represents the resistance to bending (E_b is the non-dimensional elastic bending resistance of the cilium). The second term, S, expresses the active (normal) shear generated by the sliding filaments in the cilium. We chose here

$$S(s,t) = (\pi/2)C_N\omega(L^2/S_0)(s^2 - 1)\sin[2\pi(1 - 2t)] \times c_1(t) \times c_2(s,t), \tag{12}$$

where $c_1(t)$ and $c_2(s,t)$ are the same as in G-L:

$$c_1(t) = \begin{cases} a_1 & 0 \le t \le t_1 \\ a_2 & t_1 < t \le 1, \end{cases} \tag{13}$$

and

$$c_2(s,t) = \begin{cases} 1 & 0 \le s \le 1, \quad 0 \le t \le t_1 \\ 1 & 0 \le s \le a_3 \quad t_1 \le t \le 1 \\ 0 & a_3 < s \le 1, \quad t_1 \le t \le 1. \end{cases} \tag{14}$$

We conclude that the phase shift appearing in Eq. 12 (compared to the analogous equation in G-L) is planned to restrict the motion to the first octant (i.e., $x_1, x_2, x_3 \ge 0$).

For the binormal component we also have an expression consisting of a passive bending resistance term and an active contribution denoted by $P(s,t)$:

$$F_B = E_b\kappa\tau + P(s,t). \tag{15}$$

$E_b\kappa\tau$ represents the elastic properties of the cilium if we consider it as an isotropic "beam" with "effective" bending stiffness. In Appendix C we prove this claim and refer to cases which are not isotropic.

In this paper P is defined by

$$P(s,t) = (\pi/2)C_N\omega(L^2/S_0)(S^2 - 1)\sin(2\pi t)\ c_3(t). \tag{16}$$

The function $c_3(t)$ determines the time periods where F_B is "active" and is defined as:

$$c_3(t) = \begin{cases} 0 & 0 \le t \le t_2 \\ 1 & t_2 \le t \le t_3 \\ 0 & t_3 \le t \le 1. \end{cases} \tag{17}$$

Here $(t_3 - t_2)$ is the duration of the "nonplanar" effect.

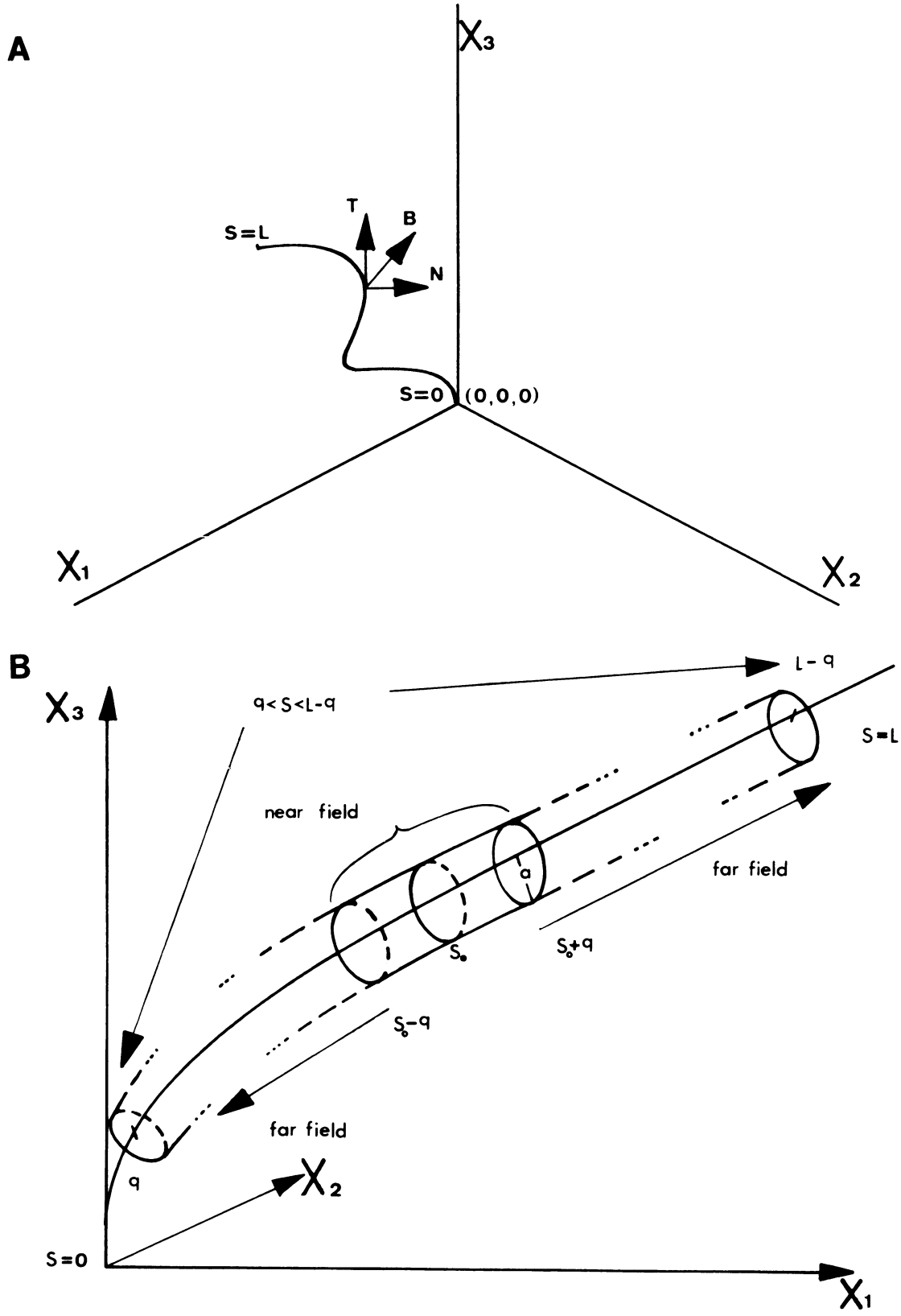

FIGURE 1 (*a*) Local, and global 3-D coordinate systems. (*b*) The near field, and the far field for a given cross section of the cilium (see Theorem 1).

Initial and boundary conditions, parameter values, and numerical procedures

Since the choice of the the initial and boundary conditions is similar to what has been done in G-L, we just mention the self-evident points briefly. All simulations start with an erect cilium (i.e., one whose centerline is aligned with the x_3 axis), for which the torsion and curvature are zero. At the anchor, the cilium points in the direction of the x_3 axis. As already concluded, whenever the curvature becomes zero, the time evolution equations for the 3-D curve are not well defined. This calls for a special treatment which will be explained later on. The boundary conditions are

$$\kappa = \tau = 0 \quad \text{at} \quad s = 0, \tag{18}$$

to maintain the initial (erect) orientation, and to keep the cilium planar and straight at the anchor and at the distal end

$$\kappa_s = \tau_s = 0 \quad \text{at} \quad s = 0 \quad \text{and at} \quad s = 1. \tag{19}$$

Other implied conditions are

$$\mathbf{V} = \boldsymbol{\phi} = 0 \quad \text{at} \quad s = 0, \tag{20}$$

$$\mathbf{F} = 0 \quad \text{at} \quad s = 0 \quad \text{and} \quad s = 1 \tag{21}$$

and(note that these last two equations are vectorial equations).

The equations that are used in the model are Eqs. B2–B5, 6–8, and 10–21. A straightforward approach to a numerical-computing procedure, which is the easiest to follow, is the explicit one. Starting with the values of κ and τ at a certain time, the normal and binormal components of the shear force (F_N, F_B) can be obtained from Eqs. 11–17. Eq. 10 is then applied to calculate F_T. With the three components of $\mathbf{F}$ known, ϕ_N, ϕ_T, and ϕ_B are computed by using the force balance equation (Eq. B2), and its derivatives (Eqs. B3–B5). Theorem 1, Eqs. 3 and 4, relating the drag force to the velocity, yields a vectorial integral equation with the unknown variables V_T, V_N, and V_B. As in the 2-D case, it can be solved iteratively. Knowing the velocity components, we can use the geometric propagation Eqs. 6–8. These equations form a system of coupled nonlinear differential equations.

The above explicit approach turns out to be inadequate. It yields stability problems (as indicated in H-B for example) and thus necessitates the use of an unreasonably small time step. There are many alternative methods for solving such nonlinear PDE systems. Generally, the instability problems can be avoided by using implicit schemes, which then allow for larger time steps. Mixed strategies, where explicit schemes are used for some of the terms, and implicit schemes for the more problematical terms (e.g., Ref. 6) can also be applied. We opted to use the Crank-Nicolson algorithm, combined with an iterative approach, in order to overcome these numerical difficulties (the same way as for the 2-D model, see G-L and H-B). The difference from the 2-D case is that here a nonlinear *system* of equations (propagating the curvature *and* the torsion) must be solved at each step (instead of the single equation, propagating only the curvature in the 2-D model). After discretization, this system, becomes a *coupled system of nonlinear algebraic equations*, to which Newton-Raphson's method was applied. However, despite the resemblance between the 2-D and the 3-D models, the latter requires much greater computational efforts. The reason is that, in order to assure the convergence of Newton's iterative method, the time step must be decreased to a much smaller value than what was sufficient for the 2-D case.

The instances where the cilium became straight (i.e., $\kappa = 0$ at one or more points on the cilium, and thus the equations become singular) had to be treated differently. In practice, it occurred only at the beginning of the beat cycles, where the cilium returned to its initial erect position, thus its tangent at this position was $\mathbf{x}_3$ (a unit vector in the direction of the x_3 axis). Since in such events there is no "intrinsic" normal, we assigned $\mathbf{x}_1$ (a unit vector in the direction of the x_1 axis) as one. The curve was treated as planar (in the x_1–x_3 plane) for several time steps and the curvature could then be propagated by using Eq. 6, with the torsion equal to zero. This was enough to "fold" the cilium back to a position where the set of Eqs. 6–8 became applicable again.

To conclude, we list the values of the parameters as follows: $L = 10$ μm, $a = 0.1$ μm (chosen to fit typical cilia dimensions); $S_0 = 10^{-12}$ newton (a typical force magnitude, see H-B); $E_b = 25 \cdot 10^{-24}$ newton m^2 (as in H-B); $\omega = 25$ Hz (a typical beat frequency). Modeling the engine, the following parameters were used: $a_1 = 2$, $a_2 = 2$, $a_3 = 1$, $t_1 = 1$, $t_2 = 0.25$, $t_3 = 0.25$. Finally, the spatial and time steps for the numerical schemes were: $dt = 0.002$, i.e., 500 time steps/one beat cycle. $ds = 1/50$, i.e., 51 discretization points on each cilium. (It was verified that decreasing ds and dt does not give significantly different results.)

RESULTS

This section summarizes the results of the simulations and briefly describes the use of the animated-display technique we used. All the results reported here, are for the periodic beat pattern (usually obtained within five cycles).

Results for one cilium

Choosing the parameters specified in the Modeling section, beat patterns that simulated the two distinct phases of the cycle (the effective and recovery strokes) were obtained. During the effective stroke the cilium is almost straight and planar. During the recovery stroke it starts folding "sideways," out of the plane of the effective stroke. Next, it straightens up, back to the initial erect position. Variations on this basic pattern can be obtained by altering the parameters of the internal mechanism. This demonstrates the flexibility of our model. The beat patterns produced by the simulations, resemble beats that are observed experimentally (31, 23). A typical beat pattern is presented in Fig. 2, *a* and *b*. The "snapshots" (distinct cilia positions) were taken in time intervals of 0.1 (i.e., 10 snapshots/cycle). Both figures show the same beat but from different view points.

In Fig. 2, *c–e*, we display the results for one cilium, exposed to an external shear flow: x_3 $\mathbf{x}_2$, $1.4x_3$ $\mathbf{x}_2$ and $-x_3$ $\mathbf{x}_1$, respectively. The effect of the external shear flow is felt through the term $V_{ext}(s_0,t)$ in Eq. 1. As seen in the figures, the external flow drives the cilium out of the plane during the effective stroke and generates additional bending in the appropriate direction.

Multicilia configurations

In contrast to the 2-D case, we could arrange the cilia "array" in different ways (we account for the interaction between the cilia as explained in the Preliminaries section (e.g., Eq. 3). For a more detailed description see G-L). We investigated two kinds of configurations of three cilia. The first is where the cilia were placed in a column in the direction of the effective stroke (denoted by "column configuration"). In the second configuration they were arranged in a row which was perpendicular to the direction of the effective stroke (which we denote by "row configuration"). We investigated the changes in the original beat, resulting from the interaction between neighboring cilia. More prominent changes are apparent in the column configurations. Fig. 3, *a–d*, shows snapshots of row and column (three cilia) configurations. The snapshots were taken during both the effective and the recovery strokes. The cilia were started simultaneously, with the same initial conditions (i.e., erect position) and were spaced at a normalized distance of 0.1 from each other.

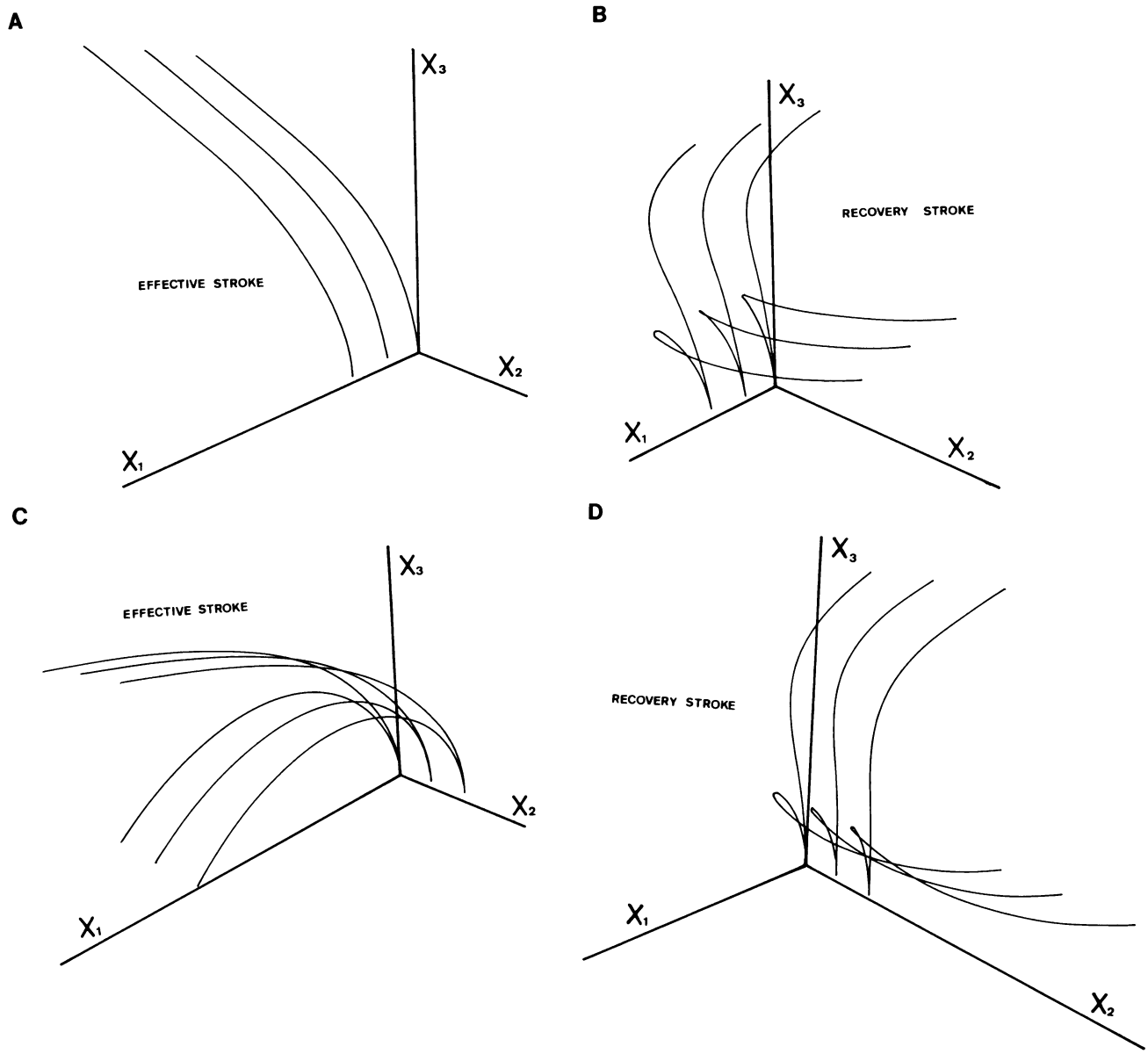

FIGURE 2 Snapshots of a beat cycle of a single cilium (10 snapshots/one beat cycle, i.e., dimensionless time intervals of 0.1). (*a*) Viewpoint (3,3,3), view direction toward the origin. (*b*) Viewpoint (3,4,5), view direction toward the origin. (*c*) Exposed to an external shear flow $x_3 \times x_2$ (viewpoint 3,3,3; view direction toward the origin). (*d*) Exposed to an external shear flow $1.4x_3 \times x_2$ (viewpoint 3,3,3; view direction toward the origin). (*e*) Exposed to an external shear flow $-x_3 \times x_1$ (viewpoint 3,3,3; view direction toward the origin).

DISCUSSION

The new equations, developed in this paper, enable simulations of 3-D cilia beats. Since most cilia have 3-D beat patterns this model represents an improved and more useful tool for realistic simulations of ciliary motion.

The 2-D beats for multicilia configurations in the 2-D case involved limited bending and tangential motion, so as to avoid cilia colliding into each other, as explained in G-L. In the 3-D case, with the effective stroke in one plane and the recovery stroke out of this plane, we achieved beats with large amplitude and also considerable tangential motion. Moreover, we had no problem in packing the cilia close together, in contrast to the 2-D case.

Our paper is chiefly aimed at the introduction of a method for simulating 3-D beats. Therefore we settled for a rather arbitrary model for the internal mechanism, and attributed simple (isotropic) elastic properties to the cilia. Finer modeling attempts that rely heavily on the internal structure and the elastic properties of the cilia can easily follow.

The computation time involved with the 3-D model is considerably larger than in the 2-D simulations. This is why we report only on simulations with a relatively small number of cilia (all simulations have been performed on an IBM PS/70 computer). For this reason the results for multicilia configurations should be considered only as a preliminary investigation. However, as we mentioned before, solving similar (geometric) problems required the use of supercomputers when other existing algorithms were used.

We conclude with a note on the enhanced displaying technique we designed for the 3-D problem. In G-L we have

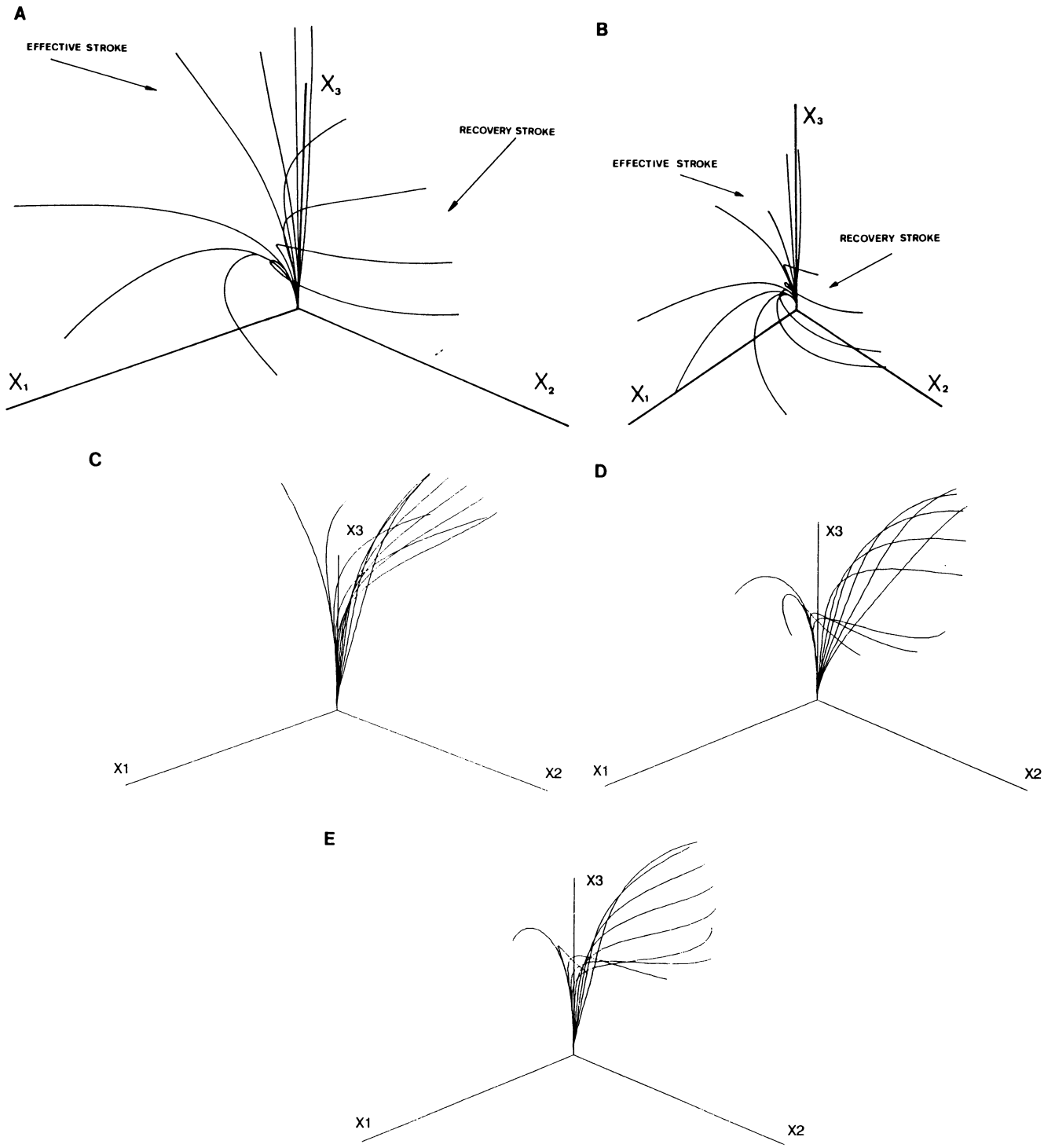

FIGURE 3 A configuration of three cilia, started with identical initial conditions. The viewpoint is 3,3,3; and the view direction is toward the origin. (*a*) Column configuration. One snapshot during the effective stroke. (*b*) Column configuration. Two snapshots during the recovery stroke. The cilia proceed from near the surface to upright position. (*c*) Row configuration. Two snapshots during the effective stroke. (*d*) Row configuration. Two snapshots during the recovery stroke. The cilia proceed from near the surface to upright position.

already discussed the fact that the ciliary beats could not be convincingly drawn. This is more the case when dealing with 3-D beats, since we cannot plot too many snapshots on the same graph. Another important investigation tool is the ability to change the view point and the view direction. This is helpful, for example, in order to determine the precise time where the cilia leave the plane of the effective stroke (by viewing them from the front). The enhanced animation program possesses all the features of the 2-D version, reported in G-L, namely: slow and fast motion control and frame-by-frame advance. Additionally, it enables the selection of view point and the view direction to be changed, thus allowing the "sacnning" of the cilia from all directions and angles. All the relevant results reported in the paper are pre-

sented in this way, and the resulting demonstration program is available upon request.

APPENDIX A

The proof of Theorem 2 (the Modeling section) follows.

Theorem

Let $V_T(s)$, $V_N(s)$, and $V_B(s)$ be the (local) velocity components of each point along an inextensible curve. The equations describing the evolution of the curvature and the torsion in time are:

$$\kappa_t = V_{Nss} + V_T\kappa_s - 2\tau V_{Bs} - \tau_s V_B + (\kappa^2 - \tau^2)V_N, \tag{A1}$$

$$\tau_t = \beta_s + \kappa(V_{Bs} + \tau V_N), \tag{A2}$$

where β is defined by

$$\beta\kappa = V_{Bss} + 2V_{Ns}\tau + V_N\tau_s + V_T\kappa\tau - V_B\tau^2. \tag{A3}$$

Proof

Start by presenting the velocity, $\mathbf{V}$, in terms of the local coordinates:

$$\mathbf{V} = V_T\mathbf{T} + V_N\mathbf{N} + V_B\mathbf{B}. \tag{A4}$$

Differentiating the location vector, $\mathbf{r}(s,t)$, twice, with respect to s and to t yields

$$\mathbf{T}_t = \mathbf{V}_s. \tag{A5}$$

As explained in the Modeling section, interchanging the order of differentiation is allowed only because the curve is inextensible.

After using Eq. 5 we obtain

$$\mathbf{T}_t = (V_{Ts} - \kappa V_N)\mathbf{T} + (V_{Ns} + \kappa V_T - \tau V_B)\mathbf{N} + (V_{Bs} + \tau V_N)\mathbf{B}. \tag{A6}$$

Since $|\mathbf{T}| = 1$, we have

$$0 = (\mathbf{T}\cdot\mathbf{T})_t = 2\mathbf{T}_t\cdot\mathbf{T}. \tag{A7}$$

Scalar multiplication of Eq. A6 by $\mathbf{T}$, using Eq. A7 yields

$$V_{Ts} - \kappa V_N = 0. \tag{A8}$$

Equation A8 is a necessary condition that must hold between the velocity components, in order to maintain inextensibility. Clearly, Eq. A8 is the same condition that was derived by H-B, while developing the 2-D geometric equations. One should note that the binormal component of the velocity does not appear in Eq. A8. The conclusion is that a binormal motion does not affect the curve's length (for an inextensible curve), which is an interesting observation in itself. Differentiating the left-hand side of Eq. A5 again, with respect to s, and applying Eq. 5 to the left-hand side (obtaining the right-hand side is straightforward) yields

$$\mathbf{T}_{ts} = (\mathbf{T}_s)_t = (\kappa\mathbf{N})_t = \kappa\mathbf{N}_t + \kappa_t\mathbf{N}. \tag{A9}$$

Since $|\mathbf{N}| = 1$, it follows that $\mathbf{N}_t\cdot\mathbf{N} = 0$. Multiplying Eq. A9 by $\mathbf{N}$ and using Eq. A8 again, we obtain Eq. A1.

Next, we develop an equation for τ_t. Differentiating Eq. A5 with respect to s yields

$$(\kappa\mathbf{N})_t = \mathbf{V}_{ss}. \tag{A10}$$

Define

$$\beta \equiv (1/\kappa)(\kappa\mathbf{N})_t\cdot\mathbf{B} = (1/\kappa)\mathbf{V}_{ss}\cdot\mathbf{B} = \mathbf{N}_t\cdot\mathbf{B}. \tag{A11}$$

Differentiating β with respect to s we obtain

$$\beta_s \equiv \mathbf{N}_{ts}\cdot\mathbf{B} + \mathbf{N}_t\cdot\mathbf{B}_s = (\tau\mathbf{B} - \kappa\mathbf{T})_t\cdot\mathbf{B} - \tau\mathbf{N}_t\cdot\mathbf{N}, \tag{A12}$$

and since $\mathbf{N}\times\mathbf{N}_t = \mathbf{B}\times\mathbf{B}_t = 0$, $|\mathbf{B}| = 1$, $\mathbf{T}\cdot\mathbf{B} = 0$, it follows that

$$\beta_s = \tau_t - \kappa\mathbf{T}_t\cdot\mathbf{B} = \tau_t - \kappa\mathbf{V}_s\cdot\mathbf{B}. \tag{A13}$$

Differentiating Eq. A4 with respect to s, using Eq. 5 and the orthogonality properties of the triplet $\mathbf{T}$, $\mathbf{N}$, and $\mathbf{B}$ we obtain

$$\mathbf{V}_s\cdot\mathbf{B} = V_{Bs} + \tau V_N, \tag{A14}$$

and Eq. A2 follows.

A straightforward calculation of (the vector) $\mathbf{V}_{ss}$, using Eq. A11, yields Eq. A3 for β.

APPENDIX B

The derivation of the Assertion (under Modeling the Internal Mechanism of the Cilia) follows.

Assertion

The inextensibility requirement dictates the following equation:

$$F_{Tss} = (1 + C_{TN})F_{Ns}\kappa + C_{TN}F_T\kappa^2 + F_N\kappa_s - C_{TN}g_N\kappa + g_{Ts} - C_{TN}\kappa\tau F_B, \tag{B1}$$

where $C_{TN} = C_T/C_N$.

Proof

The force balance equation yields the following vectorial equation

$$\mathbf{F}_s = \boldsymbol{\phi}. \tag{B2}$$

Applying the Frenet equations (Eq. 5), we obtain the following equations from the components of Eq. B2:

$$\phi_T = F_{Ts} - F_N\kappa, \tag{B3}$$

$$\phi_N = F_{Ns} + F_T\kappa - \tau F_B, \tag{B4}$$

$$\phi_B = F_{Bs} + \tau F_N. \tag{B5}$$

Finally, substituting Eqs. 4, B2, and B4 into Eq. A8 yields the desired equation (Eq. B1).

Note that for $\tau \equiv 0$ (i.e., the case where the cilium is planar), Eq. B1 reduces to its analogous planar equation in G-L.

APPENDIX C

In this appendix we derive the equations for the elastic moment:

$$F_N = E_b\kappa_s \tag{C1}$$

$$F_B = E_b\kappa\tau \tag{C2}$$

for the elastic (shear) forces that are developed in an elastic rod (i.e., a cilium with no engine) in order to maintain equilibrium. These expressions are derived under the assumptions that the rod is isotropic and is subjected to external forces (with no external torque).

Equations C1 and C2 are obtained by differentiating the expression for the elastic moment

$$\mathbf{M} = E_b\kappa\mathbf{B}, \tag{C3}$$

with respect to s. Using the Frenet equations and the equilibrium of the forces and moments (see G-L)

$$\mathbf{M}_s = \mathbf{T}\times\mathbf{F}. \tag{C4}$$

To justify Eq. C3 we follow the notations of Hines and Blum (15). We define (at each point along the cilium) a set of three orthogonal unit vectors (named body coordinates) $\mathbf{x}$, $\mathbf{y}$, $\mathbf{z}$, where $\mathbf{z}$ is a unit vector in the direction of the

neutral axis (the centerline) of the cilium (i.e., **T**). The vectors **x** and **y** are chosen in such a way that the body coordinate system is right-handed. The unit vectors **x**, **y**, and **z** change their orientation, as a function of s, in rates that are denoted κ_x, κ_y, and κ_z, respectively (that is, if the change from body coordinates at s to body coordinates at $s + ds$ is represented as successive rotations by the angles θ_x, θ_y, and θ_z about the **x**, **y**, and **z** axes, respectively, then $\kappa_x = d\theta_x/ds$, $\kappa_y = d\theta_y/ds$, and $\kappa_z = d\theta_z/ds$). Consequently, κ_x represents rotation about the **x** axis (in the **y**–**z** plane) and κ_y represents the analogous rotation about the **y** axis. κ_z, which represents rotation about the **z** axis is the twist of the cilium, and it should not be confused with its torsion (see Eq. C8, below). Linear elastic properties can be expressed with these notations by

$$M_x = E_x\kappa_x, \qquad M_y = E_y\kappa_y, \qquad M_z = E_z\kappa_z \tag{C5}$$

where E_x, E_y, E_z are the resistances to bending in the **y**–**z** and **x**–**z** planes, and to twisting about the **z** axis, respectively (22).

It can be proven (see Ref. 18 for details) that differentiation with respect to s, in body coordinates is determined by

$$\mathbf{x}_s = -\kappa_y\mathbf{z} + \kappa_z\mathbf{y}, \qquad \mathbf{y}_s = \kappa_x\mathbf{z}\ \kappa_z\mathbf{x}, \qquad \mathbf{z}_s = 0. \tag{C6}$$

With Eq. C6 and the Frenet equations one can relate κ and τ to κ_x, κ_y, and κ_z, and write **B** and **N** in body coordinates as follows:

$$\kappa = (\kappa_x^2 + \kappa_y^2)^{1/2} \tag{C7}$$

$$\tau = \kappa_z + [\arctan(\kappa_y/\kappa_x)]_s \tag{C8}$$

$$\mathbf{B} = (\kappa_y/\kappa)\mathbf{y} + (\kappa_x/\kappa)\mathbf{x} \tag{C9}$$

$$\mathbf{N} = -(\kappa_x/\kappa)\mathbf{y} + (\kappa_y/\kappa)\mathbf{x}. \tag{C10}$$

The assumption that the cilium is isotropic (e.g., due to its circular cross section and uniform material properties) implies that $E_x = E_y$, which is denoted by E_b. Zero external torque implies that κ_z vanishes. Using Eqs. C5–C10, Eq. C3 is now straightforward.

In the general case one would like to consider the internal structure of the inner filaments of the cilium, rather than settle for "effective" elastic properties. In contrast to the isotropic case, **M** will then have tangential and normal components as well according to Eqs. C6–C10. Twist (and external torque) can also be incorporated by adding appropriate terms to Eq. C4.

This research was supported by the Fund for Promotion of Research at the Technion, Israel Institute of Technology, and by a grant from the Basic Research Foundation, The Israel Academy of Sciences and Humanities.

REFERENCES

1. Brokaw, C. J. 1970. Bending moments in free-swimming flagella. *J. Exp. Biol.* 53:445–464.
2. Brokaw, C. J. 1972a. Computer simulation of flagellar movement. I. Demonstration of stable bend propagation and bend initiation by the sliding filament model. *Biophys. J.* 12:564–586.
3. Brokaw, C. J. 1972b. Computer simulation of flagellar movement. II. Influence of external viscosity on movement of the sliding filament model. *J. Mechanochem. Cell Motil.* 1:203.
4. Brokaw, C. J. 1975. Cross bridge behavior in a sliding filament model for flagella. *In* Molecules and Cell Movement. S. Inoue, and R. E. Stephens, editors. Raven Press, New York. 165–179.
5. Brokaw, C. J. 1976. Computer simulation of flagellar movement. IV. Properties of an oscillatory two-state cross-bridge model. *Biophys. J.* 16:1029–1041.
6. Brokaw, C. J. 1985. Computer simulation of flagellar movement. VI. Simple curvature-controlled models are incompletely specified. *Biophys. J.* 48:633–664.
7. Brokaw, C. J., and D. Rintala. 1975. Computer simulation of flagellar movement. Models incorporating cross-bridge kinetics. *J. Mechanochem. Cell Motil.* 3:77–86.
8. Brokaw, C. J., and D. Rintala. 1977. Computer simulations of flagellar movement. V. Oscillation of cross-bridge models with an ATP-concentration-dependent rate function. *J. Mechanochem. Cell Motil.* 4:205–227.
9. Dresdner, R. D., D. F. Katz, and S. A. Berger. 1980. The propulsion by large amplitude waves of uniflagellar micro-organism of finite length. *J. Fluid. Mech.* 97:591–621.
10. Gray, J., and G. Hancock. 1955. The propulsion of sea-urchin spermatozoa. *J. Exp. Biol.* 32:802–814.
11. Gueron, S., and N. Liron. 1992. Ciliary motion modeling, and dynamic multicilia interactions. *Biophys. J.* 63:1045–1058.
12. Higdon, J. J. L. 1979. A hydrodynamic analysis of flagellar propulsion. *J. Fluid. Mech.* 90:685–711.
13. Higdon, J. J. L. 1979. The hydrodynamics of flagellar propulsion: helical waves. *J. Fluid. Mech.* 94:331–351.
14. Higdon, J. J. L. 1979. The generation of feeding currents by flagellar motion. *J. Fluid. Mech.* 94:305–330.
15. Hines, M., and J. J. Blum. 1978. Bend propagation in flagella. I. Derivation of equations of motion and their simulation. *Biophys. J.* 23: 267–340.
16. Hines, M., and J. J. Blum. 1979. Bend propagation in flagella. II. Incorporating of dyenin cross-bridge kinetics into the equations of motion. *Biophys. J.* 25:421–442.
17. Hines, M., and J. J. Blum. 1979. Biophysics of flagellar motility. *Rev. Biophys. Quart.* 12:103–180.
18. Hines, M., and J. J. Blum. 1983. Three-dimensional mechanics of eukaryotic flagella. *Biophys. J.* 41:67–79.
19. Hines, M., and J. J. Blum. 1984. On the contribution of moment-breaking links to twisting in a three-dimensional sliding filament model. *Biophys. J.* 46:559–565.
20. Hines, M., and J. J. Blum. 1985. On the contribution of dyenin-like activity to twisting in a three-dimensional sliding filament model. *Biophys. J.* 47:705–708.
21. Johnson, R. E., and C. J. Brokaw. 1979. Flagellar hydrodynamics: a comparison between resistive-force theory and slender-body theory. *Biophys. J.* 25:113–127.
22. Landau, L. D., and E. M. Lifshitz. 1972. Theory of Elasticity. Pergamon Press, New York.
23. Machemer, H. 1972. Ciliary activity and metachronism in Protozoa. *In* Cilia and Flagella. M. A. Sleigh, editor. Academic Press, Inc., New York. 199–286.
24. Myerscough M. R., and M. A. Swan. 1989. A model for swimming unipolar Spirilla. *J. Theor. Biol.* 139:201–218.
25. Phan-Thien, N., T. Tran-Cong, and M. Ramia. 1987. A boundary-element analysis of flagellar propulsion. *J. Fluid. Mech.* 185:533–549.
26. Ramia, M. 1991. Numerical methods for the locomotion of Spirilla. *Biophys. J.* 60:1057–1078.
27. Rikmenspoel, R. 1973. The contractile mechanism in cilia. *Biophys. J.* 13:955–993.
28. Rikmenspoel, R. 1976. Contractile events in the cilia of Paramecium, Opalina mytilus and Phragmatopma. *Biophys. J.* 16:445–470.
29. Rikmenspoel, R. 1982. Ciliary contractile model applied to flagellar motion. *J. Theor. Biol.* 96:617–645.
30. Samuels, D. C., and R. J. Donnelly. 1990. Sideband instability and recurrence of Kelvin waves on vortex cores. *Phys. Rev. Lett.* 64:1385–1388.
31. Sleigh, M. A. 1962. The Biology of Cilia and Flagella. Pergamon Press, Oxford.
32. Stoker, J. J. 1969. Differential Geometry. Wiley-Interscience, New York.